Journal of Power Sources 185 (2008) 993–1000

Contents lists available at ScienceDirect

Journal of Power Sources

journal homepage: www.elsevier.com/locate/jpowsour

Effects of nickel on network structure and thermal properties of a new solid oxide cell seal glass

M.K. Mahapatra, K. Lu*

Department of Materials Science and Engineering, Virginia Polytechnic Institute and State University, Blacksburg, VA 24061, USA

ARTICLE INFO

Article history:
Received 30 July 2008
Accepted 3 September 2008
Available online 11 September 2008

Keywords:
Network structure
Connectivity
Glass transition temperature
Dilatometric softening temperature
Thermal stability

ABSTRACT

Successful seal design relies on good understanding of glass network structure and the corresponding impact on glass thermophysical properties. This study is focused on effects of nickel replacement of glass formers SiO_2 and B_2O_3 and glass modifier SrO on SrO—La_2O_3—Al_2O_3—B_2O_3—SiO_2 glass network structure and thermal properties. Glass structure local ordering was studied by Raman spectroscopy. Glass network connectivity was formulated to compare glass structure evolution with nickel addition for different compositions. Glass transition temperature and dilatometric softening temperature were evaluated by dilatometry. Glass thermal stability was studied by X-ray diffraction. Nickel behaves as a glass modifier in the studied glass system and decreases glass network connectivity. However, nickel can increase or decrease glass transition temperature and dilatometric softening temperature depending on the specific composition. Overall, nickel addition degrades glass thermal stability by increasing the amount of non-bridging oxygen atoms and devitrification.

1. Introduction

Glass and glass-ceramic are the most suitable candidates for solid oxide fuel/electrolyer cell sealing due to their thermomechanical and thermochemical advantages while metal, metal–ceramic composite, and ceramic seals all have their own limitations [1–3]. To be used as a sealant material, glass and glass-ceramic have to meet the following criteria. Glass transition temperature (T_g) should be lower than cell operating temperatures (600–850 °C). Glass softening temperature (T_d) should be high enough to avoid excessive glass flow at cell operation temperatures. Coefficient of thermal expansion (CTE) should be greater than 9.0×10^{-6} K^{-1} in order to match with other cell components, which include yttria-stabilized zirconia, stainless steel, and lanthanum manganite. Also, continuous and/or excessive devitrification of glass or glass-ceramic sealant should not occur. In addition, seals should have good chemical stability to sustain stringent reducing and oxidizing atmospheres at high temperatures for long time (50,000 h) without failure. Sealant must also be electrically insulating.

In our prior study [4,5], it has been reported that La_2O_3 and B_2O_3 in the 25SrO—20La_2O_3—7Al_2O_3—40B_2O_3—8SiO_2 glass system degrade glass thermal stability and contribute to devitrification by forming $LaBO_3$. Also, B_2O_3 decreases glass network connectivity, T_g, and T_d. Other studies suggested that B_2O_3 may even evaporate in the form of volatile HBO_2 and $B(OH)_3$ species in the presence of water steam at cell operating temperatures [6,7]. Therefore, B_2O_3 content should be as low as possible in this SrO—La_2O_3—Al_2O_3—B_2O_3—SiO_2 (SABS)-based glass.

Recently, we discovered a different SABS glass that has low B_2O_3 and La_2O_3 contents and almost all the desirable characteristics of a solid oxide cell sealing glass [8]. The glass has T_g up to 775 °C, T_d up to 815 °C, and good thermal stability. However, no knowledge exists about the role of nickel additive in this class, especially if nickel additive amount is low, such as 1–2 mol%. Nickel has been studied in other systems as an additive, but the results are ambiguous, if not contradictory. For example, in MgO—Al_2O_3—SiO_2—B_2O_3 sealing glass, addition of nickel and Cr_2O_3 as nucleating agents increases glass transition temperature T_g and devitrification temperature T_c, and changes crystallization kinetics. The nucleating agents make the sealant thermally more stable and show the potential to tailor the seal glass thermophysical properties [9,10]. In BaO—Al_2O_3—B_2O_3—SiO_2 system, NiO addition increases CTE and decreases T_g, T_c, and softening point [11]. In SrO—Y_2O_3—B_2O_3—SiO_2 systems, NiO degrades thermophysical properties by decreasing T_g and CTE [12]. Thus the role of Ni/NiO (nickel will be oxidized into NiO and this conversion is implied throughout the paper) can be opposite for different glass systems. For the newly discovered SABS glass system, the field strength of nickel ion 0.55–0.61 (0.55 when coordination number is 6 and 0.61 when coordination number is 4) falls in-between the field strength of glass network former region

* Corresponding author. Tel.: +1 540 231 3225; fax: +1 540 231 8919.
E-mail addresses: mkmanoj@vt.edu (M.K. Mahapatra), klu@vt.edu (K. Lu).

0378-7753/$ – see front matter © 2008 Elsevier B.V. All rights reserved.
doi:10.1016/j.jpowsour.2008.09.006

(1.00–2.00) and modifier region (≈0.35) [13]. It is unknown how nickel affects the SABS glass thermophysical properties and thermal stability and whether nickel ions act as a glass network former or a glass network modifier.

This study is to understand the effects of nickel replacement of glass former (SiO_2, B_2O_3) and glass modifier (SrO) on the SABS glass structure, thermophysical properties, and thermal stability. SABS glass with 0 mol% and 5 mol% B_2O_3 were studied. Nickel of 2 mol% was added to substitute either SiO_2, B_2O_3, or SrO in the same amount in order to understand the following: (1) How does nickel affect SABS glass structure and connectivity? Does nickel act as a glass modifier or a glass network former? (2) How does nickel affect SABS glass thermophysical properties such as T_g and T_d? (3) How does nickel influence SABS glass thermal stability?

2. Experimental procedure

2.1. Glass preparation

SrO—La_2O_3—Al_2O_3—B_2O_3—SiO_2-based glass samples were prepared with conventional glass manufacturing process. $SrCO_3$ (99.9%, Sigma–Aldrich, St. Louis, MO), La_2O_3 (99.98%), Al_2O_3 (99.95%), B_2O_3 (99.98%), SiO_2 (99.8%) (all oxides were from Alfa Aesar, Ward Hill, MA), and nickel metal powders (INCO powder type 110, Novamet, Wyckoff, NJ) at designed ratios were mixed in a ball mill for overnight. The mixed powders were heated in a platinum crucible in a box furnace (Lindberg, Model No. 51314, Watertown, WI) to 1100 °C and kept there for 1 h for $SrCO_3$ to decompose. After that, the mixture was heated to 1400 °C for 4 h. The heating rate was 10 °C min^{-1}. The molten glass was quenched into a graphite mold. The glass compositions in this study were abbreviated as SABS-0 and SABS-5, in which the numbers 0 and 5 indicate 0 mol% and 5 mol% B_2O_3, respectively. All the glass compositions had 40 mol% of SrO, La_2O_3, and Al_2O_3 at fixed SrO:La_2O_3:Al_2O_3 ratios. The total amount of B_2O_3 and SiO_2 was 60 mol%. The Al_2O_3 amount was 5.0 mol%. In the SABS-0 glass, 2.0 mol% nickel powder was used to replace the glass former SiO_2 or glass modifier SrO of the same amount. In the SABS-5 glass, 2 mol% nickel powder was added to replace glass former SiO_2 or B_2O_3. The formation of the SABS glasses was confirmed by X-ray diffraction (XRD) study.

2.2. Raman spectroscopy

For network structure analysis of the SABS glasses, quenched glass samples were polished to optical finish. Raman spectra of the polished samples were collected in 200–1600 cm^{-1} wave number range using a Raman spectrometer (JY Horbia LabRam HR 800, Horiba Ltd., Japan) with a CCD detector and a Labspec software package. The light source was a 514.57 nm argon laser at 50 mW power and 400 s exposure time. The spectra were later corrected to remove background noise and temperature effect [14]. For data analysis, the Raman spectra were fitted to Gaussian bands without any restriction to deconvolute the superimposed Raman peaks [15,16]. Curve fitting was done with GRAMS/AI (7.02) software (Themo Fisher Scientific, Inc. Waltham, MA).

2.3. Dilatometry

Glass transition temperature (T_g) and dilatometric softening temperature (T_d) of the SABS glass samples from room temperature to 900 °C were measured with a push-rod dilatometer (Model 1600R, The Edward Orton Jr. Ceramic Foundation, OH). Cylindrical samples of 27 mm × 5 mm were annealed before the dilatometry study in order to remove the residual stress from the glass quenching process and allow the glass structure to relax [5]. During the dilatometry study, the samples were heated at 3 °C min^{-1} heating rate to 900 °C for 2 h and then cooled to room temperature at the same rate. Each sample was thermally cycled three times under this condition.

2.4. Phase analysis

For thermal stability study, the SABS glass samples were put on a platinum foil and heated to 850 °C at the same heating and cooling rate of 5 °C min^{-1} (Lindberg, Model No. 54233, Watertown, WI). At 850 °C, different dwell time (20–200 h) was used for glass thermal treatment. X-ray diffraction studies were carried out in an X'Pert PRO diffractometer (PANalytical B.V., EA Almelo, The Netherlands) to identify the devitrified phases in the thermally treated samples. The scan rate was 0.0020° s^{-1} with Cu Kα radiation (λ = 1.5406 Å) and a nickel filter.

3. Results and discussion

3.1. Overall glass structure

Thermophysical properties and thermal stability of a glass depend on the presence of structural units, their relative arrangement, and the amount of bridging oxygen atoms [17]. These structural parameters in turn determine the glass microscopic connectivity. To understand the atomic bonding of the SABS glasses, the Raman spectra of different SABS-0 glasses are shown in Fig. 1.

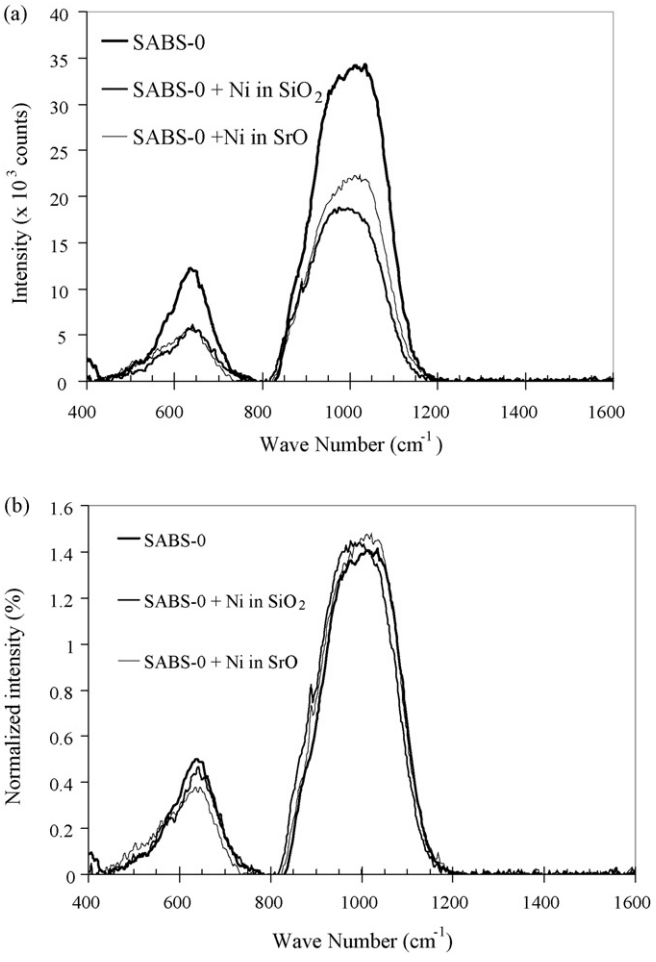

Fig. 1. Raman spectra of SABS-0 glasses: (a) as-collected, (b) normalized.

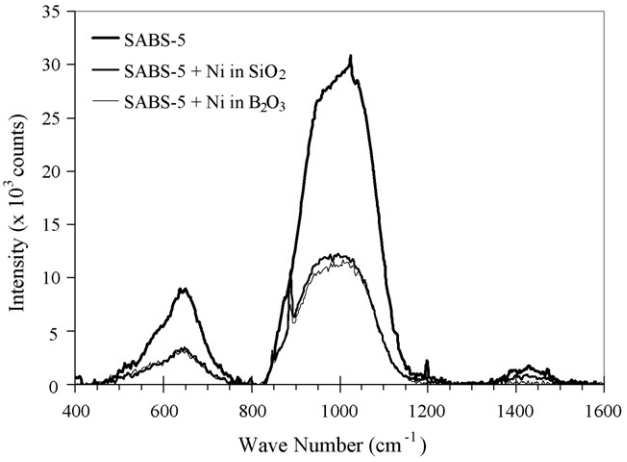

Fig. 2. Raman spectra of SABS-5 glasses.

Across 400–1200 cm^{-1} wave number range, peak intensity and peak width drastically decrease with nickel addition (Fig. 1(a)). Nickel replacement of SiO_2 has more dramatic effect on peak intensity and peak width than nickel replacement of SrO. Decreased peak width in Fig. 1(a) suggests that glass structural unit local ordering increases with nickel addition. Nickel replacement of SiO_2 has more effect on glass structure local ordering than nickel replacement of SrO. Absolute peak intensity decrease means decreased amount of structural units with nickel addition. However, relative change in peak intensity and peak width for a specific SABS glass is not directly comparable. Because of this, the Raman peaks of the three SABS-0 glasses were normalized. The normalized peaks do not show substantial peak intensity or peak width difference as shown in Fig. 1(b). This means the relative amount of different structural units in a SABS glass does not change significantly. Also, a strong peak shoulder appears around 885 cm^{-1} wave number, which will be discussed next.

Raman spectra of different SABS-5 glasses are shown in Fig. 2. Peak intensity and peak width again drastically decrease with nickel replacement of SiO_2 or B_2O_3. The peak intensity decreases slightly more for the nickel replacement of B_2O_3 case. This again means the absolute amount of the glass structural units decreases but the local ordering increases for the SABS-5 glasses. Comparison of normalized peak intensity does not show any significant change for a specific SABS-5 glass, similar to Fig. 1(b). The figure is not included for brevity. Also, nickel replacement of SiO_2 or B_2O_3 shows no change in the relative peak width. A strong peak again appears around 885 cm^{-1} wave number.

3.2. Glass structural unit local ordering

To analyze the structural unit types and distribution of the SABS glasses, it is beneficial to discuss silicate glass and borate glass structures first. In silicate glass, the 1060–1200 cm^{-1} wave number peak comes from vitreous SiO_2 with four bridging oxygen atoms. There are four major peaks representing the nature and contribution of different silicate structural units. The 1050–1100 cm^{-1} wave number peak describes the stretching motion of disilicate composition with three bridging oxygen atoms. The 950–1000 cm^{-1} wave number peak describes the stretching motion of metasilicate composition with two bridging oxygen atoms. The 900 cm^{-1} wave number peak reflects the pyrosilicate composition with one bridging oxygen atom. The 850 cm^{-1} wave number peak represents orthosilicate composition with zero bridging oxygen atom [18]. In this context the silicate units with four bridging oxygen atoms, three bridging oxygen atoms, two bridging oxygen atoms, one bridging oxygen atom, and zero bridging oxygen atom can be denoted as Q^4, Q^3, Q^2, Q^1, and Q^0, respectively. The numerals represent the number of bridging oxygen atoms that each structural unit has. The 400–700 cm^{-1} wave number peak is due to delocalized vibration of Si—O—Si bonding from mixed stretching and bending modes [18,19]. In borate glass, the 1300–1600 cm^{-1} wave number peak describes the $B—O^-$ (O^- denotes the non-bridging oxygen) stretching mode within chain and ring metaborates which also connect the network [20].

Based on the above understanding, the Raman peaks in different wave number ranges of the SABS glass spectra can be identified. However, peaks corresponding to different structural units have a tendency to overlap due to a high degree of disorder (peak widening). Also, peak frequency shift occurs for such complex glass systems [21]. To establish the correlation between the Raman peaks and specific glass structural units, the spectrum for each SABS glass sample needs to be deconvoluted. The deconvoluted spectra for the SABS-0 glass compositions are given in Fig. 3 and for the SABS-5 glass compositions are given in Fig. 4. The thick line shows the as-collected Raman spectra. The thin lines show the deconvoluted peaks from the Gaussian fitting. With the understanding that the composition difference between the conventional silicate glass and the SABS glasses can cause some peak shift, deconvoluted Raman peaks can be identified. In this study, detailed Raman spectrum analysis can be separated into three regions: 1200–1600 cm^{-1}, 800–1200 cm^{-1}, and 400–800 cm^{-1}.

3.2.1. 1200–1600 cm^{-1} region

For the SABS-0 glass, no peak is detected in the 1200–1600 cm^{-1} wave number range, corresponding to the Raman peaks from B_2O_3. This is easy to understand because the SABS-0 glass is B_2O_3 free. For the SABS-5 glass, the 1426 cm^{-1} wave number peak is from metaborate units [22]. For the SABS-5 glass with 2.0 mol% nickel replacement of SiO_2, the peak at 1426 cm^{-1} splits into three peaks at 1340 cm^{-1}, 1413 cm^{-1}, and 1457 cm^{-1}. This peak-splitting process is supported by comparing normalized areas of these peaks. The total area of the 1340 cm^{-1}, 1413 cm^{-1}, and 1457 cm^{-1} peaks match with the 1426 cm^{-1} peak area in the SABS-5 glass. The 1457 cm^{-1} peak can be assigned to localized stretching vibration of $B—O^-$ bonds in BO_3 triangles [19] or di-triborate group [23]. The 1340 cm^{-1} peak can be assigned to di-triborate group or the stretching mode of metaborates associated with non-bridging oxygen [20]. The peak splitting indicates local ordering of the metaborate structural units. For the SABS-5 glass with nickel replacement of B_2O_3, no peak is observed in the 1200–1600 cm^{-1} wave number region. This is consistent with the original spectrum in Fig. 2. Nickel replacement of B_2O_3 causes the disappearance of the $B—O^-$ stretching mode of ring and chain metaborates in the glass network. The effect of nickel addition on the SABS glass properties is similar to those of Fe^{2+} and Mn^{2+}, acting as a glass modifier [24]. In the nickel-containing SABS glasses, nickel likely forms short-range NiO_6 octahedra instead of tetrahedral arrangement. Otherwise, it should take part in glass network tetrahedral arrangement and stabilize the glass, which is not observed as to be discussed in Section 3.5. Also, nickel as a modifier in the SABS glass is confirmed by UV–vis absorption spectroscopy study. There is an absorption peak in 800–900 nm wavelength region, which suggests that nickel forms NiO_6 octahedra in the SABS glasses, in agreement with literatures [25–27].

3.2.2. 800–1200 cm^{-1} region

For the deconvoluted peaks in the 800–1200 cm^{-1} wave number range, it can be understood as follows. For the SABS-0 glass, the weak 1180 cm^{-1} and 1143 cm^{-1} wave number peaks are from the

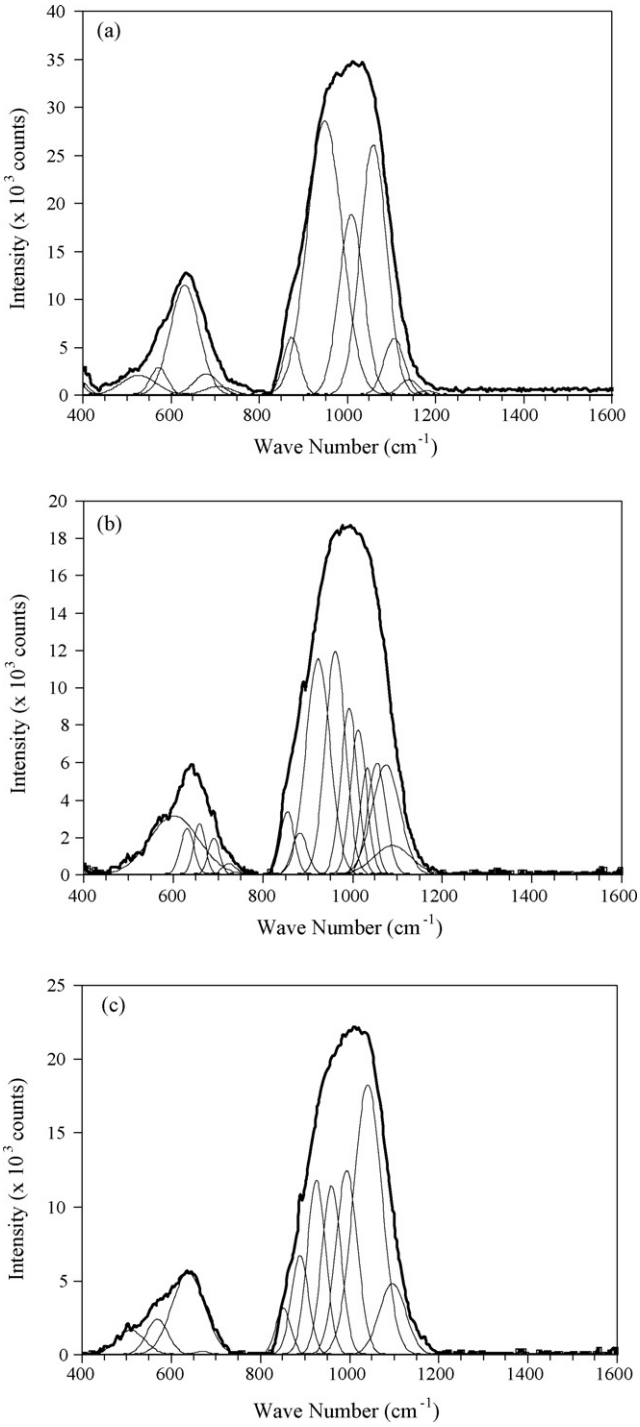

Fig. 3. Deconvoluted Raman spectra for: (a) SABS-0 glass, (b) 2 mol% nickel replacement of SiO_2 in SABS-0 glass, and (c) 2 mol% nickel replacement of SrO in SABS-0 glass.

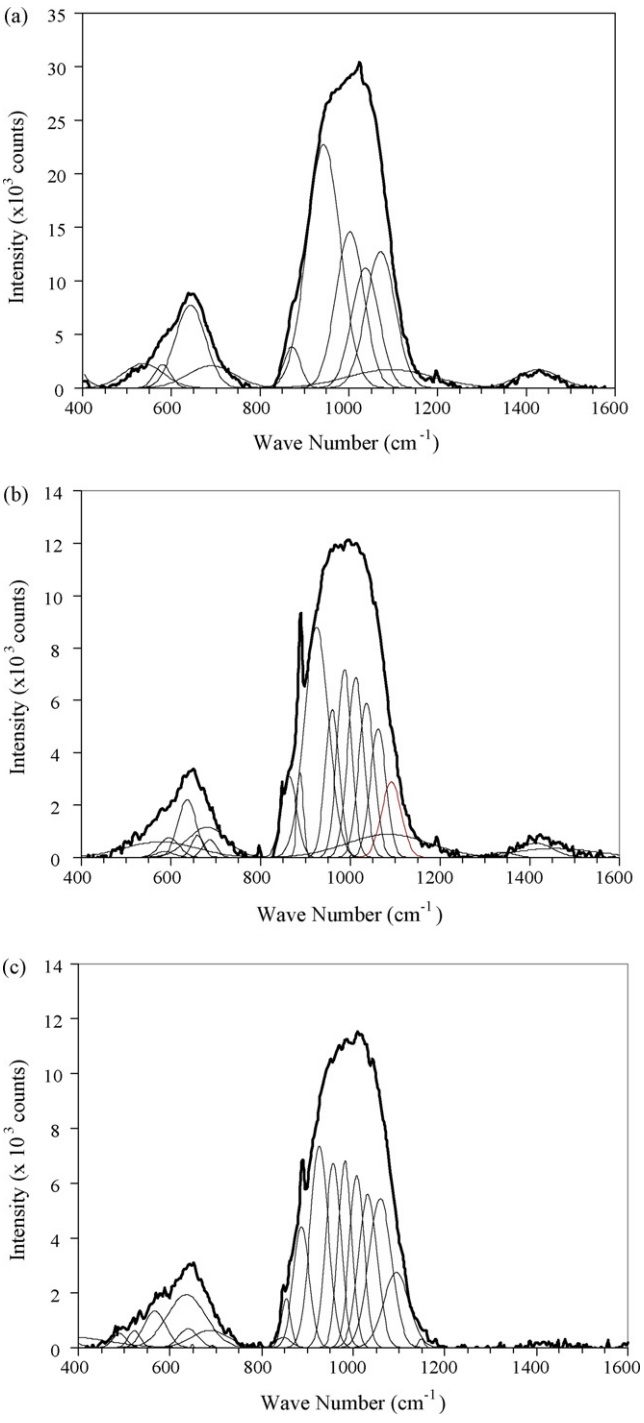

Fig. 4. Deconvoluted Raman spectra for: (a) SABS-5 glass, (b) 2 mol% nickel replacement of SiO_2 in SABS-5 glass, and (c) 2 mol% nickel replacement of B_2O_3 in SABS-5 glass.

Q^4 units [28]. The 1060 cm^{-1} and 1105 cm^{-1} wave number peaks are from the Q^3 units. The 1010 cm^{-1} and 949 cm^{-1} wave number peaks are from the Q^2 units. The 872 cm^{-1} wave number peak is from the Q^0 units [8]. This means for the SABS-0 glass, a small fraction of SiO_4 glass structure units are fully connected by bridging oxygen atoms, most of the SiO_4 glass structure units are partially connected with other SiO_4 structure units, and a small fraction of the SiO_4 glass structure units have zero bridging oxygen atoms and only coordinate with the glass modifier ions.

With 2.0 mol% nickel replacement of SiO_2 in the SABS-0 glass, the peaks corresponding to the Q^4 units are absent. The 1105 cm^{-1} wave number peak shifts to lower wave number of 1089 cm^{-1}. The 1060 cm^{-1} peak splits into four peaks: 1033 cm^{-1}, 1054 cm^{-1}, 1074 cm^{-1}, and 1089 cm^{-1} peak. The 1010 cm^{-1} peak splits into two peaks at 992 cm^{-1} and 1013 cm^{-1} wave numbers. The 948 cm^{-1} peak in the SABS-0 glass splits into two peaks at 962 cm^{-1} and 923 cm^{-1}. All these peak-splitting processes can be confirmed by peak area integration. The 923 cm^{-1} peak is attributed to discrete

$Si(OAl)_4$ units with one bridging oxygen atom [29]. A new peak at 882 cm^{-1} appears, as pointed out before. This peak is associated with discrete $Si(OAl)_4$ units with zero bridging oxygen atom, which is analogous to the 850 cm^{-1} peak in silicate glass [29]. The 855 cm^{-1} wave number peak corresponds to the Q^0 units. This Raman peak analysis shows that for the SABS-0 glass with 2 mol% nickel replacement of SiO_2, no SiO_4 structure units are fully connected to its neighboring SiO_4 units. Most of SiO_4 glass structure units are partially connected to other SiO_4 units, and a small fraction of SiO_4 glass structure units stay separated from other SiO_4 units. The Q^0 unit content increases more obviously as evidenced by the 882 cm^{-1} and 855 cm^{-1} peak appearance.

For the SABS-0 glass with 2.0 mol% nickel replacement of SrO, similar observation can be made. The 949 cm^{-1} peak splits into 994 cm^{-1}, 959 cm^{-1}, and 926 cm^{-1} peaks. This peak splitting again means increased local ordering of glass structural units. The 889 cm^{-1} peak is attributed to discrete $Si(OAl)_4$ units with zero bridging oxygen atom.

For the SABS-5 glass, no Q^4 glass structural unit is detected. The 1094 cm^{-1}, 1072 cm^{-1}, and 1037 cm^{-1} wave number peaks are from the Q^3 units. The 943 cm^{-1} wave number peak is from the Q^2 units. The 872 cm^{-1} wave number peak is from the Q^0 units. This means for the SABS-5 glass, none of the SiO_4 glass units are fully connected to other SiO_4 units. Most of the SiO_4 units are partially connected to other SiO_4 units in the glass network. Some SiO_4 units stay separated from other SiO_4 units. For the SABS-5 glass with 2 mol% nickel replacement of SiO_2, the 1072 cm^{-1} peak splits into 1091 cm^{-1}, 1084 cm^{-1}, and 1062 cm^{-1} peaks. The 987 cm^{-1}, 1003 cm^{-1}, and 1012 cm^{-1} peaks can be assigned to Q^2 units. The 943 cm^{-1} peak splits into 924 cm^{-1} and 960 cm^{-1} peaks. The 872 cm^{-1} peak splits into 863 cm^{-1} and 888 cm^{-1} peaks. This extensive peak splitting again means increased local ordering of glass structural units. For the SABS-5 glass with 2 mol% nickel replacement of B_2O_3, similar observations can be made. A weak peak appears at 1148 cm^{-1} wave number which can be assigned to the Q^4 units. The 1072 cm^{-1} peak splits into 1059 cm^{-1} and 1094 cm^{-1} peaks. The 1002 cm^{-1} peak splits into 982 cm^{-1} and 1008 cm^{-1} peaks. The 944 cm^{-1} peak splits into 926 cm^{-1} and 956 cm^{-1} peaks. The 874 cm^{-1} peak splits into 847 cm^{-1}, 857 cm^{-1}, and 887 cm^{-1} peaks. This again indicates that nickel replacement of SiO_2 and B_2O_3 in the SABS-5 glass increases glass local ordering and nickel ions act as a glass modifier.

3.2.3. 400–800 cm^{-1} region

For the SABS-0 glass, the 619 cm^{-1} and 641 cm^{-1} wave number peaks are from the Q^2 units corresponding to the characteristic bands of metasilicate glasses between 620 cm^{-1} and 640 cm^{-1} [30]. The 606 cm^{-1} wave number peak is from the broken Si—O bonds as in vitreous silica with the Q^3 units [21,31]. With nickel replacement of SiO_2, peak shifting occurs in the SABS-0 glass along with the appearance of new peaks. The 606 cm^{-1} peak shifts to 602 cm^{-1} with significantly increased integrated area. The 619 and 641 cm^{-1} peaks shift to 631 cm^{-1} and 659 cm^{-1}, respectively with decreased integrated area. The 690 cm^{-1} peak can be assigned to the Q^1 units [19,30]. A new, weak peak appears near 725 cm^{-1} wave number which can be assigned to the stretching vibrational mode of AlO_4 Q^4 units [19]. With nickel replacement of SrO, peak splitting is not clearly observed. However, new peaks appear. The 509 cm^{-1} peak is assigned to Si—O—Al linkages with four bridging oxygen atoms [19]. The 569 cm^{-1} peak is attributed to Al—O—Al bonds originating from disordering of AlO_4 and SiO_4 structural units [32]. A very weak peak at 670 cm^{-1} wave number is attributed to the Q^1 units [18,19]. Increased amount of broken Si—O bonds in the SABS-0 glass with nickel replacement of SiO_2 and disordered Al—O—Al bonds in the SABS-0 glass with nickel replacement of SrO suggest that nickel addition weakens the overall glass structure.

For the SABS-5 glass, the 642 cm^{-1} and 692 cm^{-1} wave number peaks are from the Q^2 units, the Q^1 units, and Si—O—B bonds [19]. The 537 cm^{-1} and 580 cm^{-1} wave number peaks are from BO_4 units in anionic rings [20]. With nickel replacement of SiO_2 in the SABS-5 glass, the 692 cm^{-1} peak splits into 686 cm^{-1} and 681 cm^{-1} peaks. The 642 cm^{-1} peak splits into 659 cm^{-1} and 636 cm^{-1} peaks. The 580 cm^{-1} peak splits into 596 cm^{-1}, 586 cm^{-1}, and 576 cm^{-1} peaks. The 537 cm^{-1} peak disappears. A very weak peak at 460 cm^{-1} wave number appears, which is assigned to BO_4 tetrahedra [22]. Also, the 692 cm^{-1} peak splits into 692 cm^{-1} and 687 cm^{-1} peaks. The 642 cm^{-1} peak splits into 636 cm^{-1}, 640 cm^{-1}, and 648 cm^{-1} peaks. A weak peak at 490 cm^{-1} wave number appears, which can be assigned to the broken Si—O bonds. Again, the splitting of peaks indicates the increased local ordering of the glass structural units.

Based on the Raman spectrum analysis of the nickel-containing SABS-0 and SABS-5 glasses, two conclusions can be drawn for the effect of nickel addition on the SABS glass. First, nickel addition causes Q^4 unit disappearance in SABS-0 glass and increased amount of non-bridging oxygen atoms in both SABS-0 and SABS-5 glasses. Second, the peaks correspond to the Q^2 and Q^3 units split and discrete $Si(OAl)_4$ and $Si(OAl)_4$ peaks appear, indicating increased local ordering of glass structural units and presence of micro-domain region with heterogeneous composition. From these conclusions it can be inferred that nickel acts as a glass modifier.

3.3. Glass network connectivity

Glass network connectivity indicates glass forming and retaining ability. If a glass has high connectivity, it is likely to be stable and resistant to devitrification. If a glass has low connectivity, it is likely to devitrify. Connectivity in a glass structure is determined by the number and arrangement of bridging and non-bridging oxygen bonds which link each of the building blocks to its neighbors. High amount of non-bridging oxygen atoms decreases glass connectivity. To compare SABS glass connectivity, the relative percent of different SiO_4 structural units in the 800–1200 cm^{-1} region is given in Table 1. This particular region is chosen because in the 400–800 cm^{-1} wave number region, there are mixed stretching and bending vibration mode of silicate and borate structural units. In the 1200–1600 cm^{-1} wave number region, the characteristic peaks of SiO_4 structural units are absent. The 800–1200 cm^{-1} region provides a simpler view to understand the effect of nickel addition on the glass network structure without the presence of BO_3 and BO_4 structural units.

As can be seen from Table 1, only the SABS-0 glass has significant amount of Q^4 units. The SABS-5 glass with nickel replacement of B_2O_3 has only a negligible amount of Q^4 units. The most obvious trend is increased Q^1 and Q^0 structural units in the nickel-containing SABS-0 and SABS-5 glasses. Qualitatively, this glass structural unit evolution leads to lower glass network connectivity. To quantify the glass network connectivity change with SABS glass composition, a new term, glass network connectivity (ψ), can be defined as follows based on prior knowledge of degree of network

Table 1
Relative percent of different structural units in the 800–1200 cm^{-1} region

Composition	Q^4 (%)	Q^3 (%)	Q^2 (%)	Q^1 (%)	Q^0 (%)
SABS-0	1.36	33.18	61.97		3.49
[a] SABS-0 + Ni/SiO_2		32.24	39.88	21.58	6.31
[a] SABS-0 + Ni/SrO		42.57	32.21	14.43	10.80
SABS-5		39.99	56.93		3.07
[a] SABS-5 + Ni/SiO_2		34.44	33.65	24.17	7.74
[a] SABS-5 + Ni/B_2O_3	0.23	36.62	35.53	16.27	11.36

[a] Nickel of 2 mol% replaces the same amount of corresponding oxide.

Table 2
Glass network connectivity of SABS glasses.

Composition	$\psi = \frac{\left[\sum Z_i(F_iV_i)/\sum Z_iV_i\right]_{\text{Network former}}}{\left[\sum F_iV_i/\sum V_i\right]_{\text{Network former+modifier}}}$	$\frac{\sum O^+}{\sum O^- + \sum O^+}$	Glass network connectivity, ψ (%)
SABS-0	1.400	0.531	74.31
SABS-0 + Ni/SiO_2	1.415	0.518	73.23
SABS-0 + Ni/SrO	1.385	0.519	71.84
SABS-5	1.380	0.514	70.97
SABS-5 + Ni/SiO_2	1.394	0.487	67.95
SABS-5 + Ni/B_2O_3	1.402	0.474	66.42

Table 3
Thermophysical properties of SABS glasses

Composition	T_g (°C)	T_d (°C)
SABS-0	775	815
SABS-0 + Ni/SiO_2	760	820
SABS-0 + Ni/SrO	760	810
SABS-5	710	765
SABS-5 + Ni/SiO_2	705	755
SABS-5 + Ni/B_2O_3	725	770

formation [27]:

$$\psi = \frac{\left[\sum Z_i(F_iV_i)/\sum Z_iV_i\right]_{\text{Network former}}}{\left[\sum F_iV_i/\sum V_i\right]_{\text{Network former+modifier}}} \frac{\sum O^+}{\sum O^- + \sum O^+} \quad (1)$$

F_i is the field strength of oxide i in a glass system, V_i is the amount of oxide i in vol.%, and Z_i is the atomic number of oxide i. The first term in Eq. (1) considers the bonding effect of cations that are present in a glass network. The second term represents the ratio of bridging oxygen atoms (O^+) vs. the total oxygen atoms (O^- and O^+) in a glass network. ψ represents both aspects in a glass network: bonding effect of glass network cations and the ratio of bridging oxygen atoms vs. total oxygen atoms.

It should be pointed out that from the SABS glass Raman spectra, it is not possible to determine the amount of network forming cations contributed by intermediate ion Al^{3+}. From Raman spectra, it can be seen that Al_2O_3 participates in the glass network. Since Al_2O_3 content is only 5 mol% in the SABS glass, all the Al^{3+} ions are assumed to participate in the glass network during glass network connectivity calculation. The bond strength of SiO_2, B_2O_3, Al_2O_3, La_2O_3, SrO, and NiO are 1.56, 1.62, 0.97, 0.43, 0.27, and 0.55, respectively [13]. The glass network connectivity of the SABS glasses is then calculated using Eq. (1) and the results are given in Table 2.

From Table 2, it can be seen that glass network connectivity decreases with nickel addition for both SABS-0 and SABS-5 glasses. Also, nickel replacement of SrO induces more network connectivity decrease than nickel replacement of SiO_2 for the SABS-0 glass; nickel replacement of B_2O_3 induces more network connectivity decrease than nickel replacement of SiO_2 for the SABS-5 glass. These results are consistent with the glass phase stability to be discussed in Section 3.5. Thus, Eq. (1) that quantifies glass network connectivity from deconvoluted Raman spectrum is valid. However, advanced techniques (e.g. ^{17}O NMR study) that can quantify the amount of bridging and non-bridging oxygens in a glass system will give more precise quantification of network connectivity.

3.4. Thermophysical properties

Seal glass thermophysical properties (T_g and T_d) have critical impact on glass sealing ability. T_g and T_d represent glass viscoelasticity and flowability at cell operation temperatures. From the dilatometry study, T_g and T_d values for each SABS glass sample were obtained as given in Table 3. No devitrified phase appears in the SABS samples studied by dilatometry. This indicates that the SABS glasses do not devitrify at temperatures up to 820 °C.

For the SABS-0 glass with nickel replacement of SiO_2, decrease in T_g and insignificant change in T_d are observed. Nickel replacement of SrO decreases T_g but T_d remains unchanged. Decrease in T_g is consistent with the SABS glass network structure change with nickel addition. As seen from the glass structure analysis, nickel addition hinders Q^4 unit formation, weakens the network connectivity, and decreases T_g.

When 2 mol% nickel replaces SiO_2 in the SABS-5 glass, T_g and T_d decrease by 5–10 °C. However, when nickel replaces the same amount of B_2O_3 in the SABS-5 glass, T_g increases by 15 °C and T_d increases by 5 °C. For the SABS-5 glass, decrease in T_g and T_d with nickel replacement of SiO_2 is expected because of the decrease in glass network former SiO_2, which also has high T_g and T_d values. Nickel, as a glass modifier, creates non-bridging oxygen atoms in the SABS glass and causes lower glass network connectivity. For the SABS-5 glass, increases in T_g and T_d with nickel replacement of B_2O_3 can be from higher nickel bond strength effect and reduced amount of B_2O_3. Also, the SiO_4 tetrahedra Q^4 units (1148 cm^{-1} peak in Raman spectra) reappear and this could induce higher glass connectivity in very localized regions. From these observations, it may be concluded that nickel replacement of B_2O_3 shifts the glass T_g and T_d to higher temperatures while nickel replacement of SiO_2 shifts the glass T_g and T_d to lower temperatures.

3.5. Phase evolution

Thermal stability of a seal glass is a must for solid oxide cells. The fundamental challenge is not the presence of devitrified phases, but the continuous evolution and instability of the seal glass. Excessive

Table 4
SABS glass phase evolution after different thermal treatment time at 850 °C

Sample	20 h	50 h	100 h	200 h
SABS-0	×	×	×	×
SABS-0 + Ni/SiO_2	×	×	×	t-$La_2Si_2O_7$
SABS-0 + Ni/SrO	×	×	$La_{10}Al_4O_{21}$, $La_4Sr_3O_9$	$La_{10}Al_4O_{21}$, La_2SiO_5, $SrSiO_3$, $Sr_5Al_2O_8$
SABS-5	×	×	m-$La_2Si_2O_7$, α-$SrSiO_3$, Sr_2SiO_4	Not studied
SABS-5 + Ni/SiO_2	m-$La_2Si_2O_7$, α-$SrSiO_3$	m-$La_2Si_2O_7$, $SrSiO_3$, Sr_2SiO_4	Not studied	Not studied
SABS-5 + Ni/B_2O_3	$Sr_7Al_2O_{10}$	m-$La_2Si_2O_7$, α-$SrSiO_3$, Sr_2SiO_4	Not studied	Not studied

× means the glass is amorphous.

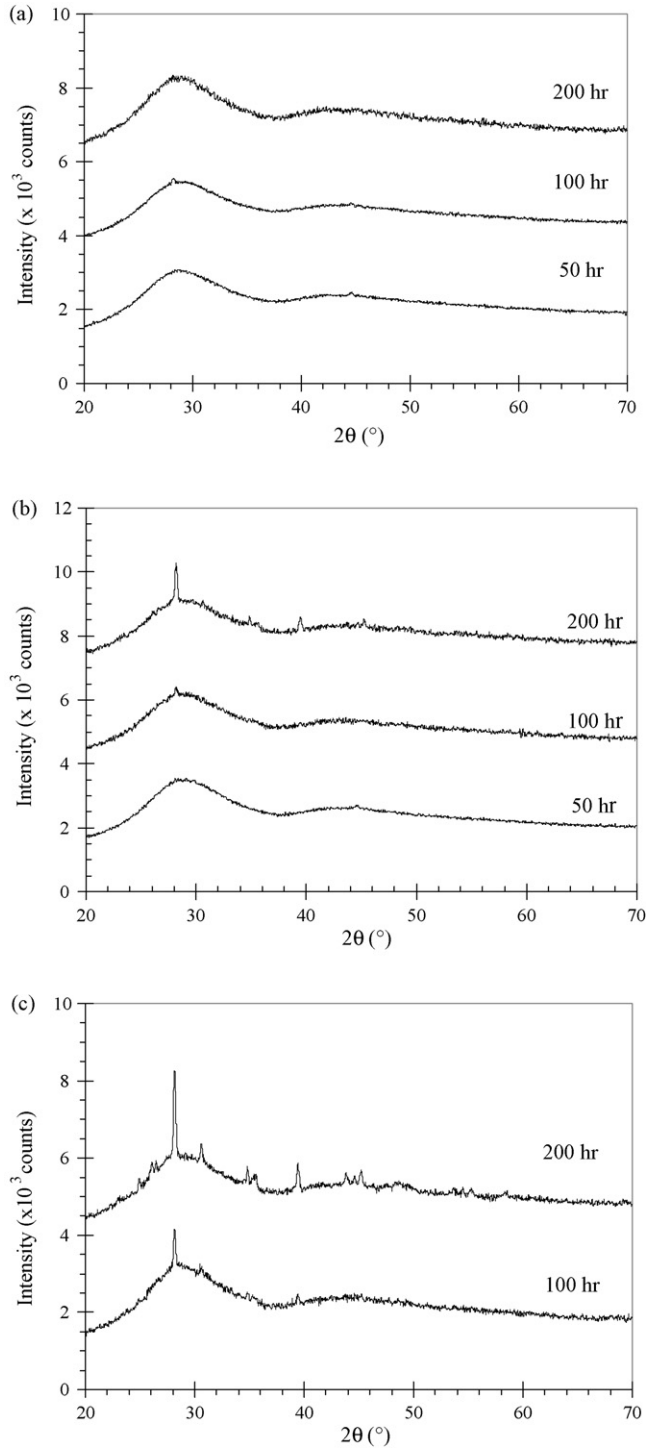

Fig. 5. XRD patterns of SABS-0 glass after thermal treatment at 850 °C for different times: (a) no nickel addition, (b) 2 mol% nickel replacement of SiO_2, and (c) 2 mol% nickel replacement of SrO.

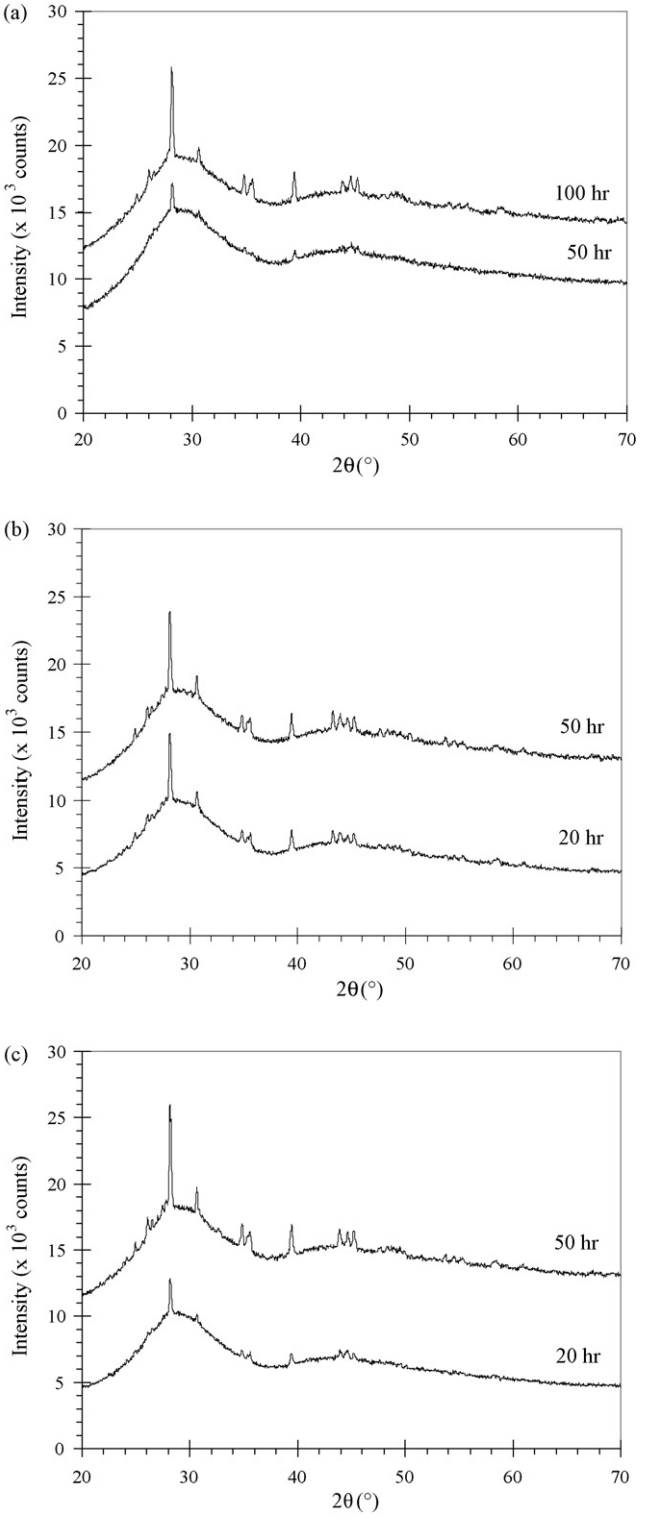

Fig. 6. XRD patterns of SABS-5 glass after thermal treatment at 850 °C for different times: (a) no nickel addition, (b) 2 mol% nickel replacement of SiO_2, and (c) 2 mol% nickel replacement of B_2O_3.

devitrification causes the glass to undesirably change from being viscous to being rigid. Sealing ability deteriorates over time and thermal stress increases because of difference in CTEs of glassy phase and devitrified phase. The end result is cracking and degradation of sealing function. In this work, XRD is used to analyze the SABS glass phase evolution with different thermal treatment time at 850 °C. Different phases are identified and given in Table 4.

As shown in Table 4, multiple phases evolve simultaneously for the same glass composition at different thermal treatment times or for different glass compositions at the same thermal treatment time. Devitrified phases that form at shorter thermal treatment time can disappear at longer thermal treatment time. One example is the $La_4Sr_3O_9$ phase for the SABS-0 glass with nickel replacement

of SrO and the other is the $Sr_7Al_2O_{10}$ phase for the SABS-5 glass with nickel replacement of B_2O_3. These phase changes suggest that the devitrified phase nucleation and growth are accompanied by decomposition reactions. Simultaneous evolution of several devitrified phases indicates that eutectic crystallization occurs in these glasses [33].

In the SABS-0 glass, no devitrified phase is detected up to 200 h of thermal treatment (Fig. 5(a)). When nickel is added to replace SiO_2, the SABS-0 glass devitrifies after 200 h of thermal treatment with the appearance of tetragonal $La_2Si_2O_7$ phase (Fig. 5(b)). The SABS-0 glass with nickel replacement of SrO devitrifies at 100 h with the appearance of $La_4Sr_3O_9$ and $La_{10}Al_4O_{21}$ phases. $La_4Sr_3O_9$ phase is metastable and disappears after 200 h of thermal treatment with the appearance of new phases La_2SiO_5, $SrSiO_3$, and $Sr_5Al_2O_8$. La, Si, Sr, and Al ions separate from the glass network and participate in devitrification. Nickel addition degrades the SABS-0 glass thermal stability by facilitating devitrification. This can be explained from the change in glass structure. Appearance of less connected structural units such as Q^1 and Q^0 enhances devitrification [34]. With nickel addition, Q^0 and Q^1 units increase in the SABS glass structure and Si—O bond breaks. Thus network connectivity of the SABS glass decreases. This is further supported by the evolution of aluminium-containing phases in the SABS-0 glass with nickel replacement of SrO, in which the Q^0 unit content is higher than that of the SABS-0 glass with nickel replacement of SiO_2. Also, portions of Q^1 and Q^0 units are composed of $Si(OAl)_4$. Micro-domains with heterogeneous composition then act as nucleation sites and induce devitrification.

The SABS-5 glass devitrifies after 50 h thermal treatment as shown in Fig. 6(a). Small devitrified peaks are observed but the intensity and number of peaks is insufficient to determine the devitrified phases. After 100 h thermal treatment at 850 °C, monoclinic $La_2Si_2O_7$ phase along with small amounts of α-$SrSiO_3$ and Sr_2SiO_4 phases appears. When 2 mol% nickel is added to replace SiO_2 (Fig. 6(b)) or B_2O_3 (Fig. 6(c)), devitrification occurs much earlier, only after 20 h of thermal treatment. For the nickel replacement of SiO_2 glass sample, the devitrified phases are monoclinic $La_2Si_2O_7$ and α-$SrSiO_3$ in contrast to the tetragonal $La_2Si_2O_7$ phase for the SABS-0 glass. For nickel replacement of B_2O_3 in the SABS-5 glass, the devitrified phase is $Sr_7Al_2O_{10}$. However, as the thermal treatment time increases to 50 h, the devitrified phases evolve into the same species as in the SABS-5 glass: $La_2Si_2O_7$, SrSiO3, and Sr_2SiO_4. $La_2Si_2O_7$ is the main phase among the three. This means nickel replacement of either SiO_2 or B_2O_3 in the SABS-5 glass exacerbates devitrification. The species that separate from the glass network are lanthanum, silicon, and strontium ions. Boron species is not involved in the devitrified phase formation. Also, $Sr_7Al_2O_{10}$ phase is thermodynamically metastable for the SABS-5 glass with 2 mol% nickel replacement of B_2O_3. Absence of Al_2O_3-containing phases in the 50 h thermally treated sample supports the observation that devitrification occurs through decomposition reactions. The devitrified phases after 50 h thermal treatment of the SABS-5 glass with 2 mol% nickel replacement of SiO_2 are also the same phases as those in the SABS-5 glass after 100 h thermal treatment. The reason for earlier devitrification with nickel addition is the same as in the SABS-0 glass. The absence of nickel in the devitrified phases suggests that nickel mainly acts as a nucleating agent during the devitrification process.

4. Conclusions

This study is focused on the effects of 2 mol% nickel replacement of glass formers SiO_2 and B_2O_3 and glass modifier SrO on SrO—La_2O_3—Al_2O_3—B_2O_3—SiO_2 (SABS) glass structure and thermal properties. Glass structural unit local ordering has been systematically studied and a new term, glass network connectivity, has been formulated. Nickel decreases SABS glass network connectivity and acts as a modifier in the glass system. Nickel replacement of SrO and SiO_2 in SABS-0 glass decreases T_g. Nickel replacement of B_2O_3 and SiO_2 in SABS-5 decreases T_g and T_d. Nickel addition in both SABS-0 and SABS-5 glasses increases devitrification tendency and decreases thermal stability. Fundamental glass structure evolution with nickel addition has been elucidated by comparing glass network connectivity of different compositions.

Acknowledgments

This material is based upon work supported by Department of Energy under Award Number DE-FC07-06ID14739. The help of Mr. Charles Farley, Department of Geoscience, Virginia Tech, during Raman spectroscopy experiment is highly appreciated. The authors also would like to acknowledge Prof. Robert Bodnar, Department of Geoscience, Virginia Tech, for his helpful suggestions during Raman spectroscopy experiment.

References

[1] J.W. Fergus, J. Power Sources 147 (2005) 46–57.
[2] P.A. Lessing, J. Mater. Sci. 42 (2007) 3465–3476.
[3] EG & G Technical Services, Fuel Cell Handbook, 7th ed., US Department of Energy, Office of Fossil Energy, National Energy Technological Laboratory, 2004.
[4] M.K. Mahapatra, C. Story, K. Lu, W.T. Reynolds Jr., Energy: Fuel Cells: Materials, Processing, Manufacturing and Power Management Technologies, in: Proceedings of the Material Science Technology, Detroit, Michigan, USA, September 16–20, 2007, pp. 371–380, Organizers: P. Singh, A.-M. Azad, D.C. Collins, P.N. Kumta, C. Legzdins, A. Manthiram, A. Manivannan, S.K. Sundaram, Z.G. Yang.
[5] M.K. Mahapatra, K. Lu, W.T. Reynolds Jr., J. Power Sources 179 (2008) 106–112.
[6] M.J. Snyder, M.G. Mesko, J.E. Shelby, J. Non-Cryst. Solids 352 (2006) 669–673.
[7] S.T. Reis, R.K. Brow, T. Zhang, P. Jasinski, Ceram. Eng. Sci. Proc. 27 (2007) 297–304.
[8] M.K. Mahapatra, K. Lu, R. J. Bodnar, Appl. Phys. A, submitted for publication.
[9] N. Lahl, K. Singh, L. Singheiser, K. Hilpert, D. Bahadur, J. Mater. Sci. 35 (2000) 3089–3096.
[10] D. Bahadur, N. Lahl, K. Singh, L. Singheiser, K. Hilpert, J. Electrochem. Soc. 151 (2004) A558–A562.
[11] S.B. Sohn, S.Y. Choi, G.H. Kim, H.S. Song, G.D. Kim, J. Am. Ceram. Soc. 87 (2004) 254–260.
[12] Y.S. Chou, J.W. Stevenson, R.N. Gow, J. Power Sources 168 (2007) 426–433.
[13] H. Scholze, Glass Nature, Structure and Properties, Springer-Verlag, New York, 1991, pp. 108–111.
[14] A.K. Hassan, L.M. Torell, L. Börjesson, H. Doweidar, Phys. Rev. B 45 (1992) 12797–12805.
[15] B.O. Mysen, L.W. Finger, D. Virgo, F.A. Seifert, Am. Mineral. 67 (1982) 686–695.
[16] H. Li, P. Hrma, J.D. Vienna, M. Qian, Y. Su, D.E. Smith, J. Non-Cryst. Solids 331 (2003) 202–216.
[17] J.E. Shelby, Introduction to Glass Science and Technology, Second ed., Royal Society of Chemistry, Cambridge, 2005, pp. 76–161.
[18] P. McMillan, Am. Mineral. 69 (1984) 622–644.
[19] E.I. Kamitoss, J.A. Kapoutsis, H. Jain, C.H. Hsieh, J. Non-Cryst. Solids 171 (1994) 31–45.
[20] R.K. Brow, D.R. Tallant, G.L. Turner, J. Am. Ceram. Soc. 79 (1996) 2410–2416.
[21] S.K. Sharma, Nature 292 (1981) 140–141.
[22] M. Środa, C. Paluszkiewicz, J. Mol. Struct. 834–836 (2007) 302–307.
[23] W.L. Konijnendijk, J.M. Stevels, J. Non-Cryst. Solids 18 (1975) 307–331.
[24] G. Calas, J. Petiau, The structure of non-crystalline materials, in: P.H. Gaskel, J.M. Parker, E.A. Davis (Eds.), Proceedings of the Second International Conference, Cambridge, UK, July 12–15, 1982, Society of Glass Technology, Taylor and Francis Ltd., London/New York, 1982, pp. 18–28.
[25] C. Nelson, W.B. White, Phys. Chem. Glasses: Eur. J. Glass Sci. Technol. B 34 (1993) 219–225.
[26] E. Cormier, L. Galoisy, G. Calas, Europhys. Lett. 45 (1999) 572–578.
[27] M.B. Volf, Chemical Approaches to Glass: Glass Science and Technology, vol. 7, Elsevier, Amsterdam, 1984, pp. 98–367.
[28] F. Seifert, B.O. Mysen, D. Virgo, Am. Mineral. 67 (1982) 696–717.
[29] P. McMillan, B. Piriou, A. Navrotsky, Geochim. Cosmochim. Acta 46 (1982) 2021–2037.
[30] B.O. Mysen, D. Virgo, F.A. Seifert, Am. Mineral. 70 (1985) 88–105.
[31] N.F. Mott, Philos. Mag. B 56 (1987) 257–262.
[32] C.I. Merzbacher, W.B. White, J. Non-Cryst. Solids 130 (1991) 18–34.
[33] D. Shi, M. Tang, M.S. Boley, M. Hash, K. Vandervoort, H. Claus, Y.N. Lwin, Phys. Rev. B 40 (1989) 2247–2253.
[34] J. Deubene, J. Non-Cryst. Solids 351 (2005) 1500–1511.